Layer Dependent Modulation of WS_2 Photoluminescence by Lateral Electric Fields

Zhengyu He,[1] Yuewen Sheng,[1] Youmin Rong,[1] Gun-Do Lee,[2] Ju Li,[3,4] Jamie H. Warner[1]*

[1]Department of Materials, University of Oxford, Parks Road, Oxford, OX1 3PH, UK

[2]Department of Materials Science and Engineering, Seoul National University, Seoul 151-742, Republic of Korea

[3]Department of Nuclear Science and Engineering, Massachusetts Institute of Technology, 77 Massachusetts Avenue, Cambridge, MA 02139, USA

[4]Department of Materials Science and Engineering, Massachusetts Institute of Technology, 77 Massachusetts Avenue, Cambridge, MA 02139, USA

*Jamie.Warner@materials.ox.ac.uk

Abstract

Large single crystal domains of WS_2 are grown by chemical vapour deposition and their photoluminescent properties under lateral electric field are studied. We demonstrate that monolayer and bilayer WS_2 have opposite responses to lateral electric fields, with lateral electric fields causing monolayer WS_2 photoluminescence (PL) to substantially reduce, whilst it increases PL in bilayer WS_2. Temperature dependent PL measurements are also undertaken and show distinctly different behaviour to the lateral electric field effects, ruling out heating as the cause of the PL changes. The PL variation in both mono- and bilayer WS_2 is attributed to the transfer of photo-excited electrons from one conduction band valley to another, modifying the resultant recombination pathways. The effect of this physical process on luminescent properties can be only observed in 2D TMDs other than bulk semiconductors, due to the much

larger exciton binding energy than the energy difference between two conduction band extrema.

KEYWORDS: WS_2, transition metal dichalcogenides, tungsten disulphide, opto-electronics, 2D crystals, Photoluminescence

Introduction

Atomically thin transition metal dichalcogenides (TMDs) are 2D materials, consisting of two hexagonal planes of chalcogen atoms X (S, Se) covalently bonded to transition metal atoms M (Mo, W) arranged hexagonally. Bulk TMDs play an important role as dry lubricants[1] and have different properties to the 2D monolayer and few layer thin films. 2D TMDs have unique electrical[2] and optical properties[3], evolving from an indirect to a direct bandgap when the number of layers decreases down to a monolayer[4,5]. The very large exciton binding energy, due to the 2D nature,[6] leads to strong excitonic photoluminescence even at room temperature[7–10]. 2D TMD materials have potential applications in a variety of opto-electronic devices, including photo-detectors[11–13], solar cells[14–17], light-emitting devices[16,18,19] and photo-transistors[20,21].

For many applications, engineering the optical properties via external modulation is highly desired [8]. Tongay *et al.*[8] reported that crossover from an indirect to a direct bandgap can be thermally driven in $MoSe_2$, where heating induced larger interlayer spacing. Strain induces lattice parameter changes and modulates the band structure, altering the optical properties of WSe_2.[22] A more desirable way to control the optical properties is through electrical manipulation. Electrostatic charging in a field effect transistor can charge the neutral exciton and produce different emission spectra[23,24]. Density functional theory (DFT) calculations also predict that sufficiently high vertical electric fields can bring the conduction and valence bands

closer, or even transform TMDs from semiconductors to zero-gap materials.[25] However, few reports have explored the optical response of TMDs under lateral electric field and during current flow, which has been proven to be an effective method to manipulate the optical properties of many other materials. Bludau *et al.*[26] and Skromme *et al.*[27] reported PL quenching from bulk GaAs and InP and attributed it to impact ionization. Similar measurements have also been carried out on low dimension materials. Zhang *et al.*[28] observed field-induced PL quenching on $Al_{0.3}Ga_{0.7}As$ /GaAs/ $Al_{0.3}Ga_{0.7}As$ single quantum wells with ultra-high time response, opening up the possibility of quantum well based high speed optical modulators. Again, impact ionization has been proposed to be the dominant quenching mechanism. Huang *et al.*[29] have reported PL switching from single colloidal quantum dots using an electric field and argued that direct exciton ionization was the dominant mechanism. Field induced PL quenching was reported for quantum nanorods, explained by the diminishing of transition matrix elememt[30].

Here we examine the changes to photoluminescence spectra from monolayer and bilayer WS_2 when a lateral electric field is applied. For monolayer WS_2, increasing lateral electric field leads to PL quenching, whilst for bilayer it causes an increase in PL emission. This finding can help fabricate more efficient optoelectronic devices[31–33] based on bilayer TMD materials. Possible mechanisms behind the PL quenching and enhancement are discussed.

Results and Discussion

Large 2D single crystals of WS_2 were grown by CVD on Si substrates with a 300 nm oxide layer, using our previously reported method[34]. This results in primarily monolayer domains, but some bilayer and few layer domains can also be found within the sample. Figure 1a shows an SEM image of the monolayer single crystal WS_2 domain with an average size of

about 100 µm. The well-defined triangular shape and uniform contrast indicate the high quality of our WS_2 samples. Monolayer and bilayer WS_2 domains can be distinguished by optical contrast if the RGB channel of the imaging CCD is optimized.[18] Figures 1b and 1c show the optical microscopy image of monolayer and bilayer isolated domains. Monolayer and bilayer are further confirmed by their PL signal, presented in figure 1d. Under same excitation laser power and CCD acquisition time, the PL integrated intensity from monolayer is 200 times stronger than that from bilayer region, arising from the evolution of electronic structure from indirect bandgap for bilayer to direct bandgap for monolayer[10,35]. Raman spectroscopy can also help in determining single layer from bilayer WS_2, shown in figure 1e. The black line represents the Raman spectrum from monolayer WS_2, showing E^1_{2g} and A_{1g} phonon modes at 352.3 cm^{-1} and 418.9 cm^{-1}. Bilayer WS_2 has a different Raman spectrum (red line in figure 1e), with E^1_{2g} blue-shifting to 351.4 cm^{-1} and A_{1g} red-shifting to 419.8 cm^{-1}, consistent with what has been previously reported.[10,36]

Figure 1f depicts the schematic diagram of the experimental setup used to monitor the PL spectra under different lateral electric field by applying source drain bias. Lithographic patterning to make electrodes to the WS_2 was avoided to ensure that no defects were introduced by the processing into the as-grown WS_2 that could influence its PL response.[24] Source-drain electrodes were made by positioning two ultrafine tungsten tips directly onto the surface of the WS_2 domains using micro-manipulators, resulting in stable contacts. The tungsten tips were typically positioned 20 µm apart underneath a long working distance objective lens in a PL confocal spectrometer. The PL was excited in the middle of the two electrodes using a 532nm laser focussed to ~2µm spot. Although the misalignment between the WS_2 conduction band and the work function of the tungsten tips can introduce a Schottky barrier, it should not influence the experiment results when considering the effect of current flow on the PL dynamics.

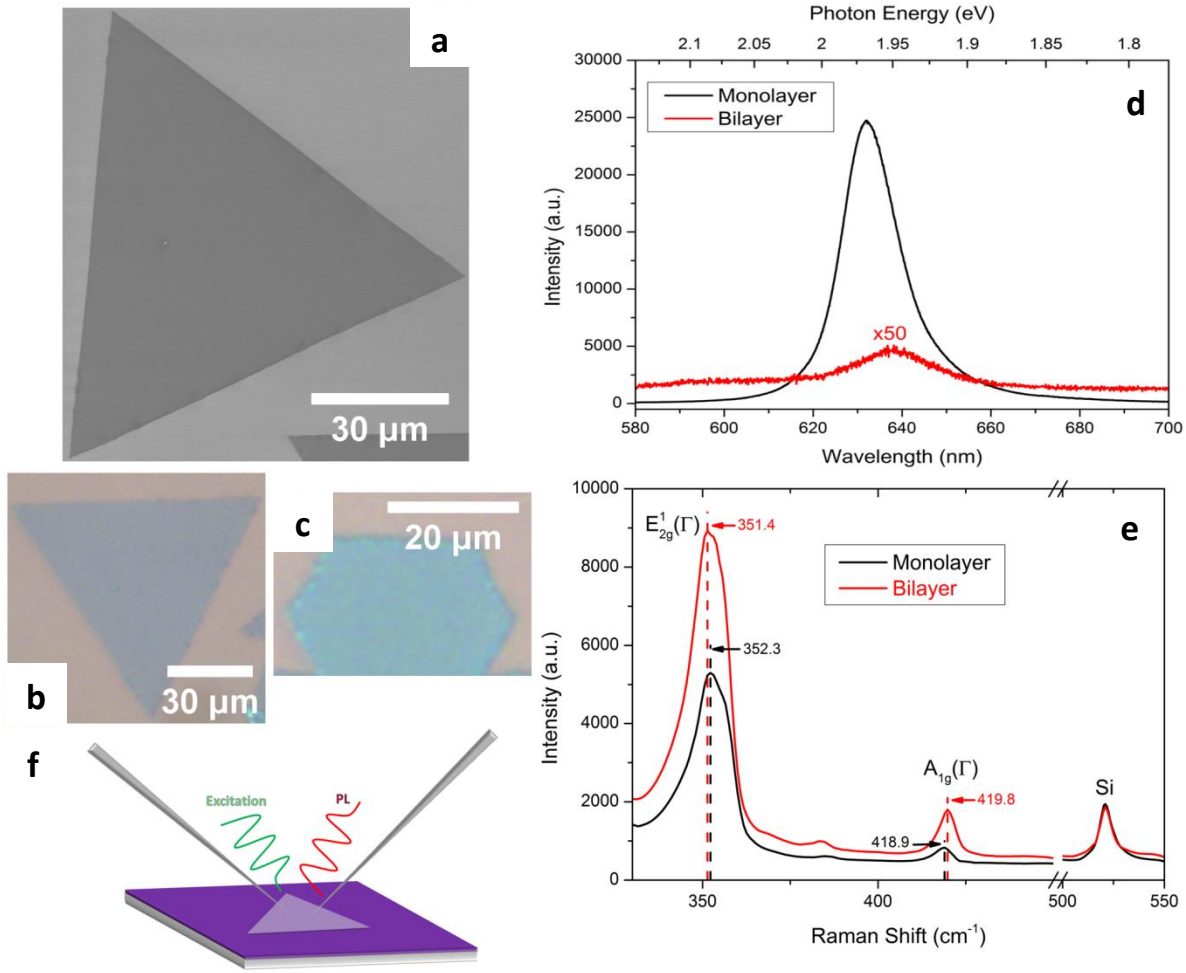

Figure 1. Identification of monolayer and bilayer WS_2. (a) SEM image of monolayer single crystal triangular shape WS_2 domain. (b,c) Optical image of (b) monolayer and (c) bilayer WS_2. (d) Photoluminescence spectra of monolayer and bilayer WS_2. (e) Raman spectra of monolayer and bilayer WS_2. Black line: monolayer. Red line: bilayer. (f) Schematic diagram of the setup used in experiment to measure PL under lateral electric field.

Figures 2a and 2b show the typical PL behaviour of monolayer WS_2 under an external lateral electric field by applying source-drain bias. We repeated these measurements on numerous monolayer crystals, which all showed the same behaviour. Under low electric field, minimal current flows and the PL changes little. However, when the electric field exceeds certain value, such as 1 kV/cm in this case, the intensity of PL starts to decrease dramatically up to 50% of the original value as the electric field continues to increase. It also shows reversible behaviour

in which the PL intensity can almost goes back to the original value as the electric field returns to zero. This indicates that the PL quenching observed under electric field is not caused by permanent structural change or chemical reaction with species in the air. In addition to PL quenching effect, another feature shown in figures 2a and 2b is the small redshift of PL spectra under electric field, which will be discussed in detail in next section. Figures 2c and 2d show both the traces of PL integrated intensity and source drain current versus lateral electric field. The nonlinearity of the I-V curve arises from the Schottky barrier, which is the result of misalignment between the work function of source-drain electrode and WS_2 conduction band[37]. In figure 2e, we plot the trace of PL integrated intensity versus source drain current, trying to find the correlation between current and PL intensity. With minimal current flow, PL intensity shows fluctuation within a small range, which is then followed by drastic quenching process. With current increasing continuously, the quenching rate decreases gradually.

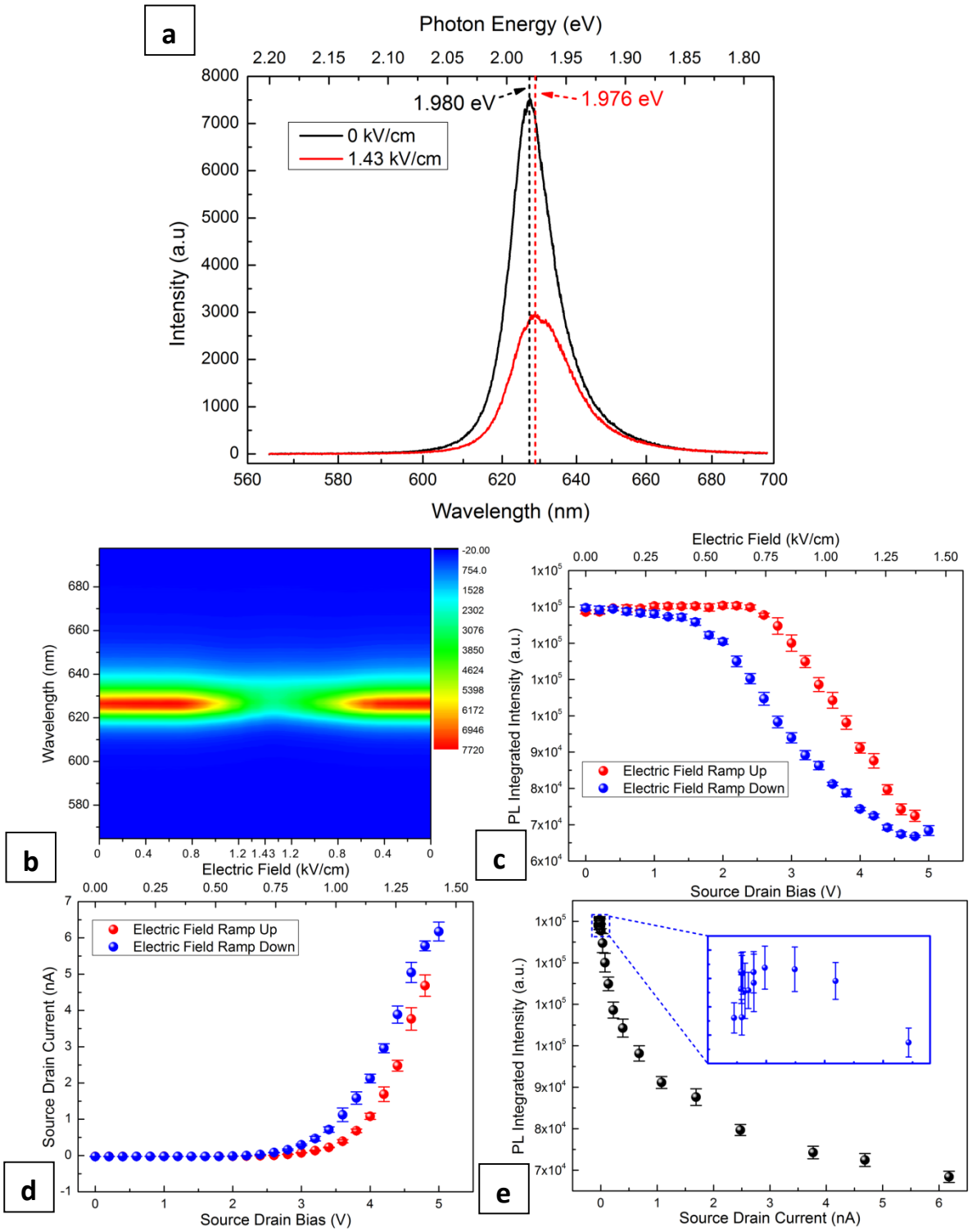

Figure 2. PL of monolayer WS_2 under lateral electric field. (a) Typical PL spectra under two different electric field, 0 kV/cm and 1.43 kV/cm. Quenching effect and redshift can be clearly observed. (b) Colour contour map of PL spectra under lateral electric field. (c) PL integrated intensity versus electric field. (d) I-V trace under laser illumination. Red balls: electric field ramps up. Blue balls: electric field

ramps down. e) Correlation between PL integrated intensity and source drain current during the process of source drain bias ramping up. Inset: magnified image of area labelled in blue rectangle.

The behaviour of bilayer WS_2 under lateral electric field is completely different to the monolayer case, with the PL greatly enhanced under lateral electric field, as illustrated in the PL spectra in figure 3a and contour colour map in figure 3b. Similar to the monolayer case, the PL intensity does not change much under weak electric field, where the current is small. As the field strengthens to certain threshold value (2.0 kV/cm in this case) the PL signal starts increasing substantially up to 150% of the original value. We have repeated these measurements on more than 10 different samples to confirm the consistency of the behaviour, and the highest value of PL increase we achieved amongst various samples measured was 300% of the original value for a large electric field (See supporting information figure S1). Again, the reversibility of this behaviour eliminates the possibility of permanent structural change or chemical reaction caused by electric field and subsequent current flowing through the material. Apart from intensity changes, the electric field also redshifts and broadens the PL peak. Figure 3c plots the PL integrated intensity versus electric field, enabling us to explore the PL intensity change into details. A noteworthy phenomenon is that PL first undergoes quenching if the electric field reaches a threshold value (1.25 kV/cm in this case) prior to enhancement. Such coexistence of both quenching and enhancement indicates two competing mechanism behind the PL change. The I-V relationship is plotted in figure 3d, where the nonlinearity is attributed to the Schottky barrier between W electrode and WS_2. Figure 3e shows the correlation between PL intensity and source drain current. It starts with fluctuations within limited range under very small current flow. The increasing current first concurs with PL quenching and then followed by enhancement. The enhancement rate slows down and stabilizes at constant value with ascending current.

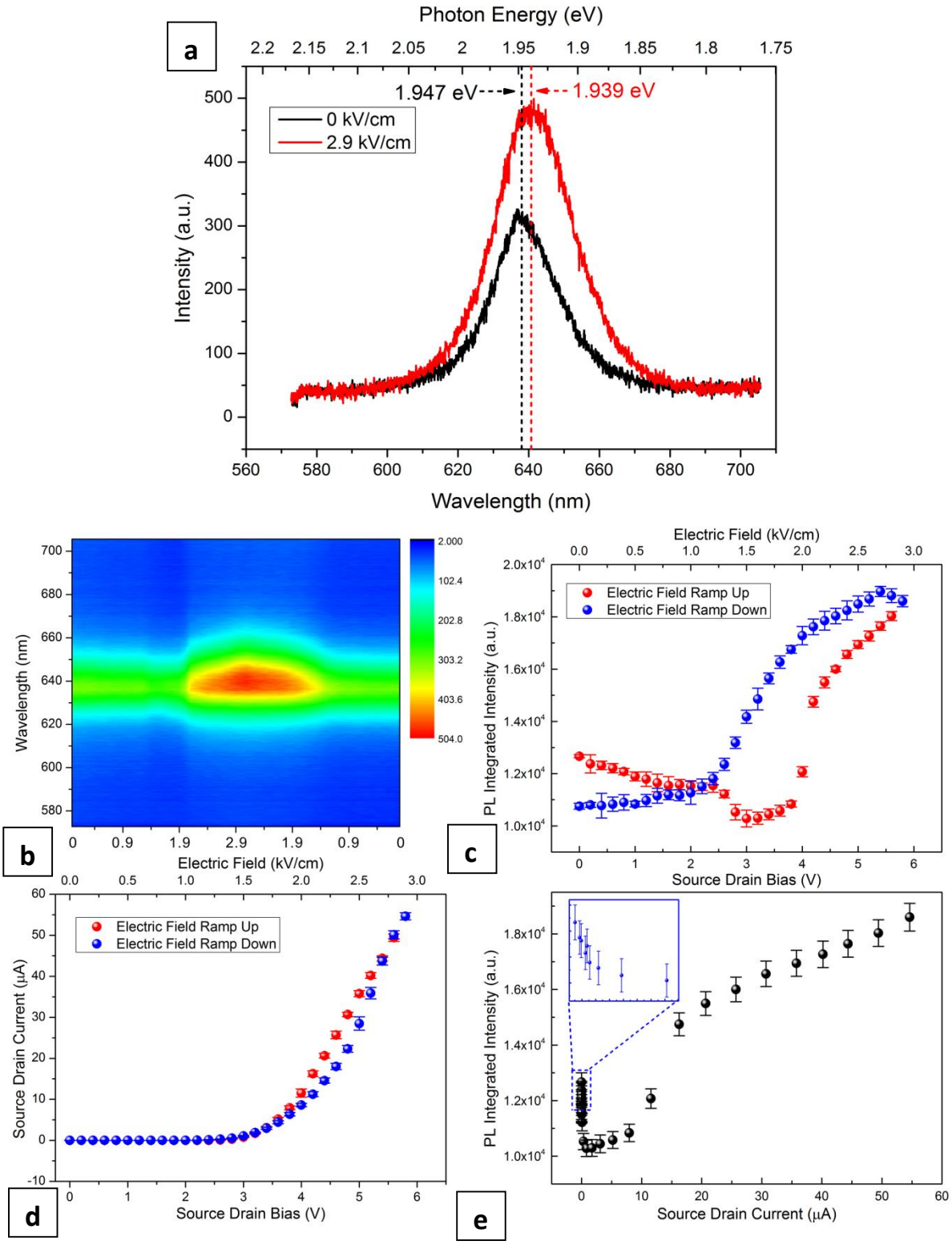

Figure 3. PL signal from bilayer WS_2 under different lateral electric field. (a) Typical PL spectra under an electric field of 0 kV/cm and 2.9 kV/cm. PL enhancement and redshift are observed. It should be pointed here that the PL we monitored comes from K-K direct recombination. (b) Colour contour map of PL spectra under lateral electric field. (c) PL integrated intensity versus electric field. (d) I-V trace

under laser illumination. Red balls: electric field ramps up. Blue balls: electric field ramps down. e) Correlation between PL integrated intensity and source drain current during the process of source drain bias ramping up. Inset: magnified image of area labelled in blue rectangle.

We measured how the PL changes for monolayer and bilayer WS_2 as a function of temperature in order to explore whether joule heating is the cause for the observed PL effects. Prior work on $MoSe_2$ showed that high temperature quenched the PL of monolayer $MoSe_2$ while it enhanced the PL of multilayer $MoSe_2$[8]. Figures 4a and 4b show the temperature dependent PL of monolayer WS_2. Clearly, figure 4a indicates that rising temperature quenches the PL dramatically by about 40% of the room temperature intensity. This quenching effect can be easily understood since the non-radiative electron-hole recombination rate increase exponentially with increasing temperature.[38] However, increasing temperature of the bilayer domain decreased the PL to ~48% of the original intensity shown in figure 4c and 4d, opposite to what we have observed for WS_2 bilayers under electric field in figure 3. We repeated these measurements more than 10 times on different samples to ensure their consistency and validity. Therefore, there must be another mechanism responsible for the PL enhancement of bilayer WS_2 induced by electric field. Along with quenching, the PL peaks in both monolayer and bilayer WS_2 experiences a large redshift with increasing temperature, as illustrated in figure 4b and 4d. Such behaviour is similar to the response of conventional semiconductors under high temperature, which is the result of increased electron-phonon interactions and slight changes in bonding lengths. Thus it provides a method to evaluate the temperature of a semiconductor.[39] By employing a standard expression for the dependence of the semiconductor bandgap versus temperature[40], it is possible to obtain the expression for exciton emission energy as a function of temperature, as in equation [1][41]:

$$E(T) = E_0 - S\langle\hbar\omega\rangle\left[\coth\left(\frac{\langle\hbar\omega\rangle}{2k_BT}\right) - 1\right] \qquad [1]$$

where E_0 is the emission energy at zero absolute temperature, S is a dimensionless coupling constant and $\langle \hbar\omega \rangle$ is the average phonon energy. At room temperature for monolayer WS_2, the best fitting yields E_0=2.08 eV, S =2.47, and $\langle \hbar\omega \rangle$= 13.0 meV and for bilayer E_0=1.97 eV, S =2.70, and $\langle \hbar\omega \rangle$= 10.8 meV. With the help of this expression, it is possible to derive the temperature difference of WS_2 under different electric fields by comparing the emission energy difference[39]. In figures 2a and 3a, the emitted photon energy shifts 4 meV for monolayer and 8 meV for bilayer, towards the low energy region, corresponding to a temperature rise of 15 K and 29 K, respectively. Such a temperature change can only yield a PL intensity suppression of about 6.0% for monolayer and 6.5% for bilayer, which is much smaller than the PL variations observed in figures 2 and 3. Therefore, it is unlikely that temperature effects are the dominant factor causing changes in the electric field dependent PL measurements.

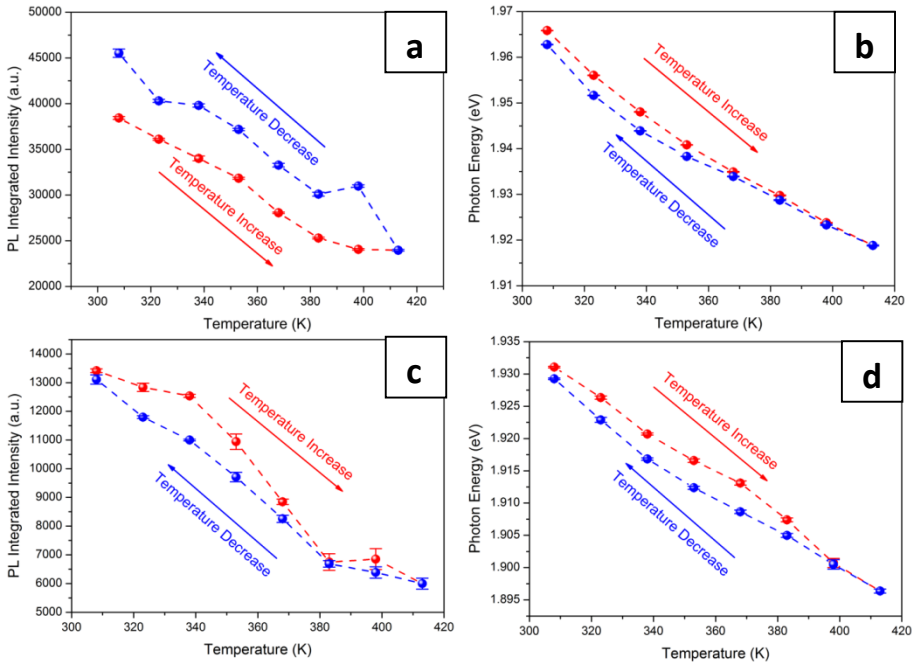

Figure 4. Temperature dependent PL of WS_2. (a-b) monolayer. (c-d) bilayer. (a,c) PL integrated intensity VS temperature. (b,d) PL photon energy VS temperature. Red line: temperature increase. Blue line: temperature decrease.

We now discuss various mechanisms that can lead to PL variation under electric field. According to previous reports, possible causes of PL quenching include: a) thermal effects[8], b) Auger decay[42], c) direct exciton ionization[29] and d) impact ionization[26,27]. Mechanism a), thermal effect, can be excluded here because we performed the temperature dependent PL measurement and showed this cannot account for the observed PL changes under electric field. For mechanism b), Auger decay, it has been shown to limit electroluminescent emission ability of LEDs[42], but it is only significant under very high carrier densities[42,43], especially for wide bandgap semiconductor.[44] Yet CVD prepared WS_2 is usually slightly n-doped for both monolayer and bilayer crystals.[45] Therefore, Auger decay is unlikely to be the main factor resulting in quenching. To clarify the validity of mechanism c), where excitons are separated apart directly by an applied electric field, it is necessary to calculate the exciton ionization threshold field strength, which is approximately given by the ratio $\frac{E_{ex}}{e \cdot a_{ex}}$, where E_{ex} is the binding energy of exciton, e is the charge unit and $a_{ex} = \frac{m_0}{\mu}\epsilon_r a_B$ is the exciton radius where m_0 is electron rest mass, μ is reduced effective mass of exciton, ϵ_r is the relative dielectric constant and a_B is Bohr radius[46]. Since the applied electric field is along the in-plane direction, we only need to consider the in-plane component of these parameters. For monolayer WS_2, E_{ex}=0.28 eV[47], μ_{xy} = 0.16m_0[47], $\epsilon_{r,xy} = 13$.[47] This yields a threshold electric field of about 6×10^5 V/cm which is 2 orders of magnitude higher than the experiment value (~10^3 V/cm, figure 2b and 2c). For bilayer, The exciton binding energy of bilayer WS_2 is about half of that of monolayer WS_2[6,18] while the reduced mass and dielectric constant changes little[6]. Hence the threshold field strength of direct exciton ionization is about 10^5 V/cm, which is still too high compared with that used in our experiment (1.25×10^3 V/cm, figure 3b and 3c). Therefore, direct exciton ionization is unlikely to account for the electric field induced quenching we observe. In mechanism d), impact ionization, carriers are first accelerated by an external field and then impact excitons generated by photon absorption. When the kinetic energy of charge

carriers is high enough, they can ionize the photo-generated excitons through the collision process, which modifies the resultant PL recombination pathways. One important criterion is that the energy of the electrons must exceed the exciton binding energy. According to our calculations, the average energy of photo-excited electrons gained under an electric field of 10^3 V/cm is about 82 meV, much lower than the exciton binding energy (Detailed calculations are presented in supporting information S2). Although there is a possibility that the energy of a very small amount of electrons may exceed the binding energy due to the energy distribution, it is unlikely to be the main contributor to PL quenching. Therefore, impact ionization is not the dominant factors to PL quenching in monolayer. In the bilayer case, although the binding energy (0.14 eV) is still higher than the average electron energy (55 meV), the smaller difference may lead to higher possibility of impact ionization of excitons, but resulting in only a small amount of PL quenching (about 10%). In order to understand the mechanism behind the quenching in the monolayer case, it is essential to figure out the parameters that determine the photoluminescence intensity, which can be expressed as[46]:

$$I(\hbar\omega) \propto |M|^2 g(\hbar\omega) \times \text{level occupancy factors} \qquad [2]$$

in which $I(\hbar\omega)$ is the luminescence intensity, $|M|^2$ is matrix element, $g(\hbar\omega)$ is joint density of states and level occupancy factors describe the probabilities that the relevant upper level is occupied by electrons and the lower level is occupied by holes. Since $g(\hbar\omega)$ is determined only by the material and layer number, it remains unchanged. $|M|^2$ is the overlap integral of the wave functions of the electron and hole, which will change little due to the small effect of the electric field on excitons with large binding energy. Therefore, only the decrease in the level occupancy factors of the K-K direct recombination pathway is likely to lead to the PL quenching. Electrons in an n-type semiconductor with two conduction band extremum can transfer from the first extremum to a secondary one under an electric field[48,49], and we propose

that the quenching in figure 2 can possibly originate from the intervalley transfer of photo-excited electrons from the conduction band minimum K valley point to the secondary extremum (middle point between K and Γ), which, therefore, modify the electrons distribution between these two conduction band extremum and decrease the level occupancy factors of K-K direct recombination pathway. The energy difference between two extrema is about 70 meV[50] (derived from DFT calculated band structure), comparable to the average energy of photo-excited electrons under electric field. Negative differential resistance is absent here, which we attribute to the very close electron effective mass between these two conduction band extrema.[48] A similar phenomenon can also help explain the PL enhancement in bilayer WS_2. The joint density of states $g(\hbar\omega)$ changes little and the matrix element $|M|^2$ decreases. Therefore, only the increase in level occupancy factors can lead to the PL enhancement, which is again the result of intervalley transfer of the photo-excited electrons from the conduction band minimum (middle point between gamma and K) to the secondary extremum (K point), which, therefore, increase the level occupancy factors of K-K direct recombination pathway. We have also calculated the average energy of electrons accelerated by electric field (71 meV), which is comparable with the energy difference between two extrema (85 meV).[51]

Conclusion

In summary, the application of lateral electric field leads to the modulation of the optical properties of WS_2. Photoluminescence from monolayer can be quenched while the emission ability of bilayer can be enhanced. Intervalley electron transfer is proposed to be the possible dominant mechanism behind the field dependent PL variations. This is due to the unique band structure (small energy difference between two conduction band extrema) and the very large exciton binding energy in 2D WS_2. In conventional bulk semiconductors it is very hard to observe the effect of this physical process on the luminescent properties because the energy difference between the conduction band extrema is much larger than exciton binding energy.[52]

These results not only shed light on understanding the very fundamental exciton behaviour of WS_2 under lateral electric fields, but also provide insights into the fabrication of TMDs based high performance optoelectronic devices and optical modulator.

Methods:

Synthesis of WS_2:

WS_2 monolayer and bilayer are prepared using our previously reported CVD method with sulphur and WO_3 as the precursor.[34] Sulphur and WO_3 are placed in a 1 inch quartz tube running through two furnace systems to provide two heating sections. Vaporized sulphur and WO_3 are carried by flowing argon gas to the reaction zone, where WO_3 undergoes sulphurization. High quality and large area WS_2 domains with atomic layer thickness are grown on Si wafers with 300 nm SiO_2 if proper parameters including temperature, Ar flow rate, sulphur introduction time are achieved.[34]

PL and Electrical Measurement:

In the photoluminescence (PL) measurement, a 532 nm diode-pumped solid state laser was for excitation, with powers kept to <200 μW. The laser reflected by a dichroic beam splitter and focused to a spot size of 2μm by 50x ultra-long working distance objective in electric field dependent measurements or a 10x objective lens in the temperature dependent measurement on to WS_2 single crystal. PL spectra were then collected through home-built confocal imaging system and the emission from the WS_2 was coupled into Princeton Instruments Acton SP-2300 spectrometer with an attached CCD (Princeton Instruments, PIXIS 100).

In the electrical measurements, two ultra-fine W tips (Signatone, SE-T, 5 um in diameter) were used to make direct contact with WS_2 crystals to avoid any damages or impurities introduction during patterning process[24]. Electrical signals were powered and measured by a Keithley source

meter (2400-LV). Both PL and electrical measurements are carried out under ambient condition and room temperature.

Acknowledgements

JHW thanks the Royal Society for support. ZH thanks the CSC and the Oxford-China scholarship fund for support.

References:

1. Kim, Y.; Huang, J.-L.; Lieber, C. M. Characterization of Nanometer Scale Wear and Oxidation of Transition Metal Dichalcogenide Lubricants by Atomic Force Microscopy. *Appl. Phys. Lett.* **1991**, *59*, 3404–3406.

2. Radisavljevic, B.; Radenovic, A.; Brivio, J.; Giacometti, V.; Kis, A. Single-Layer MoS_2 Transistors. *Nat. Nanotechnol.* **2011**, *6*, 147–150.

3. Mak, K. F.; Lee, C.; Hone, J.; Shan, J.; Heinz, T. F. Atomically Thin MoS_2: A New Direct-Gap Semiconductor. *Phys. Rev. Lett.* **2010**, *105*, 136805.

4. Li, T.; Galli, G. Electronic Properties of MoS_2 Nanoparticles. *J. Phys. Chem. C* **2007**, *111*, 16192–16196.

5. Lebègue, S.; Eriksson, O. Electronic Structure of Two-Dimensional Crystals from Ab Initio Theory. *Phys. Rev. B* **2009**, *79*, 115409.

6. Cheiwchanchamnangij, T.; Lambrecht, W. R. L. Quasiparticle Band Structure Calculation of Monolayer, Bilayer, and Bulk MoS_2. *Phys. Rev. B* **2012**, *85*, 205302.

7. Splendiani, A.; Sun, L.; Zhang, Y.; Li, T.; Kim, J.; Chim, C.-Y.; Galli, G.; Wang, F. Emerging Photoluminescence in Monolayer MoS_2. *Nano Lett.* **2010**, *10*, 1271–1275.

8. Tongay, S.; Zhou, J.; Ataca, C.; Lo, K.; Matthews, T. S.; Li, J.; Grossman, J. C.; Wu, J. Thermally Driven Crossover from Indirect toward Direct Bandgap in 2D Semiconductors: $MoSe_2$ versus MoS_2. *Nano Lett.* **2012**, *12*, 5576–5580.

9. Tonndorf, P.; Schmidt, R.; Bottger, P.; Zhang, X.; Borner, J.; Liebig, A.; Albrecht, M.; Kloc, C.; Gorden, O.; Zahn, D. R. T.; *et al.* Photoluminescence Emission and Raman Response of Monolayer MoS_2, $MoSe_2$, and WSe_2. *Opt. Express* **2013**, *21*, 4908–4916.

10. Gutiérrez, H. R.; Perea-López, N.; Elías, A. L.; Berkdemir, A.; Wang, B.; Lv, R.; López-Urías, F.; Crespi, V. H.; Terrones, H.; Terrones, M. Extraordinary Room-Temperature Photoluminescence in Triangular WS_2 Monolayers. *Nano Lett.* **2013**, *13*, 3447–3454.

11. Perea-López, N.; Elías, A. L.; Berkdemir, A.; Castro-Beltran, A.; Gutiérrez, H. R.; Feng, S.; Lv, R.; Hayashi, T.; López-Urías, F.; Ghosh, S.; *et al.* Photosensor Device Based on Few-Layered WS_2 Films. *Adv. Funct. Mater.* **2013**, *23*, 5511–5517.

12. Lopez-Sanchez, O.; Lembke, D.; Kayci, M.; Radenovic, A.; Kis, A. Ultrasensitive Photodetectors Based on Monolayer MoS_2. *Nat. Nanotechnol.* **2013**, *8*, 497–501.

13. Perea-López, N.; Lin, Z.; Pradhan, N. R.; Iñiguez-Rábago, A.; Laura Elías, A.; McCreary, A.; Lou, J.; Ajayan, P. M.; Terrones, H.; Balicas, L.; *et al.* CVD-Grown Monolayered MoS_2 as an Effective Photosensor Operating at Low-Voltage. *2D Mater.* **2014**, *1*, 011004.

14. Feng, J.; Qian, X.; Huang, C.-W.; Li, J. Strain-Engineered Artificial Atom as a Broad-Spectrum Solar Energy Funnel. *Nat. Photonics* **2012**, *6*, 866–872.

15. Wi, S.; Kim, H.; Chen, M.; Nam, H.; Guo, L. J.; Meyhofer, E.; Liang, X. Enhancement of Photovoltaic Response in Multilayer MoS_2 Induced by Plasma Doping. *ACS Nano* **2014**, *8*, 5270–5281.

16. Lopez-Sanchez, O.; Alarcon Llado, E.; Koman, V.; Fontcuberta i Morral, A.; Radenovic, A.; Kis, A. Light Generation and Harvesting in a Van Der Waals Heterostructure. *ACS Nano* **2014**, *8*, 3042–3048.

17. Bernardi, M.; Palummo, M.; Grossman, J. C. Extraordinary Sunlight Absorption and One Nanometer Thick Photovoltaics Using Two-Dimensional Monolayer Materials. *Nano Lett.* **2013**, *13*, 3664–3670.

18. Jo, S.; Ubrig, N.; Berger, H.; Kuzmenko, B. A.; Morpurgo, F. A. Mono- and Bilayer WS_2 Light-Emitting Transistors. *Nano Lett.* **2014**, *14*, 2019–2025.

19. Sundaram, R. S.; Engel, M.; Lombardo, A.; Krupke, R.; Ferrari, A. C.; Avouris, P.; Steiner, M. Electroluminescence in Single Layer MoS_2. *Nano Lett.* **2013**, *13*, 1416–1421.

20. Zhang, W.; Huang, J.-K.; Chen, C.-H.; Chang, Y.-H.; Cheng, Y.-J.; Li, L.-J. High-Gain Phototransistors Based on a CVD MoS_2 Monolayer. *Adv. Mater.* **2013**, *25*, 3456–3461.

21. Yin, Z.; Li, H.; Jiang, L.; Shi, Y.; Sun, Y.; Lu, G.; Zhang, Q.; Chen, X.; Zhang, H. Single-Layer MoS_2 Phototransistors. *ACS Nano* **2011**, *6*, 74–80.

22. Desai, S. B.; Seol, G.; Kang, J. S.; Fang, H.; Battaglia, C.; Kapadia, R.; Ager, J. W.; Guo, J.; Javey, A. Strain-Induced Indirect to Direct Bandgap Transition in Multilayer WSe_2. *Nano Lett.* **2014**, *14*, 4592–4597.

23. Mak, K. F.; He, K.; Lee, C.; Lee, G. H.; Hone, J.; Heinz, T. F.; Shan, J. Tightly Bound Trions in Monolayer MoS_2. *Nat. Mater.* **2013**, *12*, 207–211.

24. Ross, J. S.; Wu, S.; Yu, H.; Ghimire, N. J.; Jones, A. M.; Aivazian, G.; Yan, J.; Mandrus, D. G.; Xiao, D.; Yao, W.; *et al.* Electrical Control of Neutral and Charged Excitons in a Monolayer Semiconductor. *Nat. Commun.* **2013**, *4*, 1474.

25. Ramasubramaniam, A.; Naveh, D.; Towe, E. Tunable Band Gaps in Bilayer Transition-Metal Dichalcogenides. *Phys. Rev. B* **2011**, *84*, 205325.

26. Bludau, W.; Wagner, E. Impact Ionization of Excitons in GaAs. *Phys. Rev. B* **1976**, *13*, 5410–5414.

27. Skromme, B. J.; Stillman, G. E. Impact Ionization of Excitons and Shadow Donors in InP. *Phys. Rev. B* **1983**, *28*, 4602–4607.

28. Zhang, S. K.; Santos, P. V.; Hey, R. Photoluminescence Modulation by High-Frequency Lateral Electric Fields in Quantum Wells. *Appl. Phys. Lett.* **2001**, *78*, 1559–1561.

29. Huang, H.; Dorn, A.; Nair, G. P.; Bulović, V.; Bawendi, M. G. Bias-Induced Photoluminescence Quenching of Single Colloidal Quantum Dots Embedded in Organic Semiconductors. *Nano Lett.* **2007**, *7*, 3781–3786.

30. Rothenberg, E.; Kazes, M.; Shaviv, E.; Banin, U. Electric Field Induced Switching of the Fluorescence of Single Semiconductor Quantum Rods. *Nano Lett.* **2005**, *5*, 1581–1586.

31. Baugher, B. W. H.; Churchill, H. O. H.; Yang, Y.; Jarillo-Herrero, P. Optoelectronic Devices Based on Electrically Tunable P-N Diodes in a Monolayer Dichalcogenide. *Nat. Nanotechnol.* **2014**, *9*, 262–267.

32. Pospischil, A.; Furchi, M. M.; Mueller, T. Solar-Energy Conversion and Light Emission in an Atomic Monolayer P-N Diode. *Nat. Nanotechnol.* **2014**, *9*, 257–261.

33. Ross, J. S.; Klement, P.; Jones, A. M.; Ghimire, N. J.; Yan, J.; Mandrus, D. G.; Taniguchi, T.; Watanabe, K.; Kitamura, K.; Yao, W.; *et al.* Electrically Tunable Excitonic Light-Emitting Diodes Based on Monolayer WSe_2 P-N Junctions. *Nat. Nanotechnol.* **2014**, *9*, 268–272.

34. Rong, Y.; Fan, Y.; Leen Koh, A.; Robertson, A. W.; He, K.; Wang, S.; Tan, H.; Sinclair, R.; Warner, J. H. Controlling Sulphur Precursor Addition for Large Single Crystal Domains of WS_2. *Nanoscale* **2014**, *ASAP*.

35. Zhao, W.; Ghorannevis, Z.; Chu, L.; Toh, Mm.; Kloc, C.; Tan, P.-H.; Eda, G. Evolution of Electronic Structure in Atomically Thin Sheets of WS_2 and WSe_2. *ACS Nano* **2013**, *7*, 791–797.

36. Berkdemir, A.; Gutiérrez, H. R.; Botello-Méndez, A. R.; Perea-López, N.; Elías, A. L.; Chia, C.-I.; Wang, B.; Crespi, V. H.; López-Urías, F.; Charlier, J.-C.; *et al.* Identification of Individual and Few Layers of WS_2 Using Raman Spectroscopy. *Sci. Rep.* **2013**, *3*, 1755.

37. Fang, H.; Tosun, M.; Seol, G.; Chang, T. C.; Takei, K.; Guo, J.; Javey, A. Degenerate N-Doping of Few-Layer Transition Metal Dichalcogenides by Potassium. *Nano Lett.* **2013**, *13*, 1991–5.

38. Schubert, E.; Gessmann, T.; Kim, J. *Light Emitting Diodes*; Cambridge University Press, 2006.

39. Konig, U. L. F.; Langmann, U. Temperature Distribution in Gunn Diodes and GaAs MESFET ' S Determined by Micro-Photoluminescence. *Trans. Electron Devices* **1978**, *ED-25*, 49–55.

40. O'Donnell, K. P.; Chen, X. Temperature Dependence of Semiconductor Band Gaps. *Appl. Phys. Lett.* **1991**, *58*, 2924–2926.

41. Mitioglu, A. A.; Plochocka, P.; Jadczak, J. N.; Escoffier, W.; Rikken, G. K. J. A.; Kulyuk, L.; Maude, D. K. Optical Manipulation of the Exciton Charge State in Single-Layer Tungsten Disulfide. *Phys. Rev. B* **2013**, *88*, 245403.

42. Iveland, J.; Martinelli, L.; Peretti, J.; Speck, J. S.; Weisbuch, C. Direct Measurement of Auger Electrons Emitted from a Semiconductor Light-Emitting Diode under Electrical Injection: Identification of the Dominant Mechanism for Efficiency Droop. *Phys. Rev. Lett.* **2013**, *110*, 177406.

43. Kulyuk, L.; Dumcehnko, D.; Bucher, E.; Friemelt, K.; Schenker, O.; Charron, L.; Fortin, E.; Dumouchel, T. Excitonic Luminescence of the Br2-Intercalated Layered Semiconductors 2H-WS2. *Phys. Rev. B* **2005**, *72*, 075336.

44. Green, M. A. *Solar Cells: Operating Principles, Technology and System Applications*; Prentice Hall, 1982.

45. Zhang, Y.; Zhang, Y.; Ji, Q.; Ju, J.; Yuan, H.; Shi, J.; Gao, T. Controlled Growth of High-Quality Monolayer WS_2 Layers on Sapphire and Imaging Its Grain Boundary. *ACS Nano* **2013**, *7*, 8963–8971.

46. Fox, M. *Optical Properties of Solids*; Oxford Univeristy Press, 2001.

47. Chernikov, A.; Berkelbach, T. C.; Hill, H. M.; Rigosi, A.; Li, Y.; Aslan, O. B.; Reichman, D. R.; Hybertsen, M. S.; Heinz, T. F. Exciton Binding Energy and Nonhydrogenic Rydberg Series in Monolayer WS_2. *Phys. Rev. Lett.* **2014**, *113*, 076802.

48. K., R. B.; B., W. T. The Possibility of Negative Resistance Effects in Semiconductors. *Proc. Phys. Soc.* **1961**, *78*, 293–304.

49. Gunn, J. B. MICROWAVE OSCILLATIONS OF CURRENT IN III-V SEMICONDUCTORS. *Solid State Commun.* **1963**, *1*, 88–91.

50. Kang, J.; Tongay, S.; Zhou, J.; Li, J.; Wu, J. Band Offsets and Heterostructures of Two-Dimensional Semiconductors. *Appl. Phys. Lett.* **2013**, *102*, 012111.

51. Zhao, W.; Ribeiro, R. M.; Toh, M.; Carvalho, A.; Kloc, C.; Castro Neto, A. H.; Eda, G. Origin of Indirect Optical Transitions in Few-Layer MoS_2, WS_2, and WSe_2. *Nano Lett.* **2013**, *13*, 5627–5634.

52. Smith, D. L.; Pan, D. S.; McGill, T. C. Impact Ionization of Excitons in Ge and Si. *Phys. Rev. B* **1975**, *12*, 4360–4366.

TOC Graphic